The Journal of Molecular Diagnostics, Vol. 28, No. 5, May 2026

ELSEVIER

the Journal of Molecular Diagnostics
jmdjournal.org

Long-Read Whole-Transcriptome Sequencing and Selective Gene Panel Profiling Enable Sensitive Detection of Fusion Oncogenes in Pediatric B-Cell Acute Lymphoblastic Leukemia

John Lin,[*] Kofi B. Opoku,[*†] Mark R. Litzow,[‡] Elisabeth Paietta,[§] Ching-Hon Pui,[¶] Sima Jeha,[¶] Kathryn G. Roberts,[‖] Charles G. Mullighan,[‖] Thomas B. Alexander,[**††] and Jeremy R. Wang[*†††‡‡]

From the Departments of Genetics, Pediatrics,** and Pathology and Laboratory Medicine,[‡‡] School of Medicine, and the Lineberger Comprehensive Cancer Center,[††] University of North Carolina at Chapel Hill, Chapel Hill, North Carolina; Hackensack Meridian Health,[†] JFK University Medical Center, Hackensack, New Jersey; the Division of Hematology and Transplant Center,[‡] Mayo Clinic Rochester, Rochester, Minnesota; the Department of Oncology,[§] Montefiore Medical Center, Bronx, New York; and the Departments of Oncology[¶] and Pathology,[‖] St. Jude Children's Research Hospital, Memphis, Tennessee*

Accepted for publication January 14, 2026.

Address correspondence to Jeremy R. Wang, Ph.D., University of North Carolina at Chapel Hill, Brinkhous-Bullitt Bldg., 160 Medical Dr., Chapel Hill, NC 27514.
E-mail: jeremy_wang@med.unc.edu.

Long-read whole-transcriptome sequencing (WTS) has the potential to precisely characterize fusion oncogenes that drive leukemia and other cancers. Although there is a variety of general-purpose fusion detection algorithms that use modern long-read sequencing data, they show poor sensitivity for precision diagnostics in B-cell acute lymphoblastic leukemia (B-ALL) and do not robustly assess technical and analytical parameters (eg, sequencing depth) to reliably detect fusion transcripts. FUSILLI (FUSions In Leukemia Long-read sequencing Investigator) is a novel long-read fusion detection algorithm, with a focus on targeted genomic subtyping in B-ALL. FUSILLI was evaluated against extant methods using nanopore WTS from 51 pediatric B-ALL samples sequenced at high depth and 68 at low depth (mean of 11.2 and 1.4 million reads, respectively). In the high-depth cohort, FUSILLI demonstrated increased sensitivity (0.81) compared with FusionSeeker, JAFFAL, and LongGF (0.63, 0.76, and 0.70, respectively), while maintaining high specificity (0.92). At lower sequencing depth, FUSILLI showed correspondingly lower sensitivity (0.27) but still outperformed the other fusion callers (sensitivities ranging from 0.09 to 0.16). Computational down sampling suggests that 10 million reads is sufficient to sensitively detect B-ALL–relevant fusions using this approach. FUSILLI detects B-ALL fusions with high sensitivity at modest sequencing depth, supporting implementation of nanopore WTS as a low-cost and globally accessible sequencing-based molecular diagnostic platform for pediatric B-ALL and other fusion-driven cancers. *(J Mol Diagn 2026, 28: 406–421; https://doi.org/10.1016/j.jmoldx.2026.01.007)*

Acute lymphoblastic leukemia (ALL) is the most common cancer among children aged 0 to 14 years.[1] B-cell acute lymphoblastic leukemia (B-ALL) accounts for 80% of cases.[2] Current treatment of B-ALL is stratified on the basis of risk classification, which depends on age, white blood cell count, response to therapy, central nervous system status, and genomic subtype.[3] Pediatric B-ALL is primarily driven by gross karyotype abnormalities or structural variants, which typically result in fusion oncogenes. For example, the Philadelphia chromosome (Ph) results from the translocation of chromosomes 9 and 22 [t(9;22)(q34;q11)], leading to the *BCR*::*ABL1* gene fusion product.[4] Patients with B-ALL and the *BCR*::*ABL1* fusion are considered high risk and treated

Supported by the National Cancer Institute of the NIH under award numbers R01CA293366 (J.R.W.), R21CA259926 (T.B.A.), U10CA180820 (C.G.M.), UG1CA232760 (M.R.L.), and UG1CA189859 (E.P.); and National Institute of General Medical Sciences predoctoral training grant T32GM135123 (J.L.). Institutional and biobanking support was provided by UNC Lineberger Comprehensive Cancer Center, the University Cancer Research Fund, Hyundai Hope on Wheels, and Reelin' for Research.

The content is solely the responsibility of the authors and does not necessarily represent the official views of the NIH.

https://doi.org/10.1016/j.jmoldx.2026.01.007

with tyrosine kinase inhibitors and chemotherapy. In contrast, high hyperdiploid (>50 chromosomes) subtypes have a favorable prognosis when treated with standard chemotherapy regimens.[5]

The fifth edition of the World Health Organization's Classification of Haematolymphoid Tumours recognizes 13 categories of precursor B-cell neoplasms, including recent additions of gene fusion subtypes, such as *TCF3*::*HLF*.[6] However, there is no definitive list of B-ALL gene fusion subtypes as the diversity of B-ALL gene fusions continues to grow with advances in next-generation sequencing (NGS). For example, Iacobucci et al[7] show >30 ALL genomic subtypes were identified through NGS. The most common pediatric B-ALL gene fusion subtypes include *ETV6*::*RUNX1* (which occurs in 25% of cases and has excellent prognosis), followed by *TCF3*::*PBX1* (5% of cases, good prognosis) and *BCR*::*ABL1* (5% of cases, poor prognosis).[7,8]

It is critical to diagnose B-ALL genomic subtypes for appropriate risk-stratified treatment. In most centers, complete clinical classification of B-ALL requires a series of different assays, including peripheral blood smears, immunophenotyping (flow cytometry and immunohistochemistry), cytogenetics (fluorescence *in situ* hybridization and karyotyping), and targeted molecular genetics assays.[9,10]

NGS offers an alternative approach to these current methods, potentially obviating the need for multiple, complex, and time-consuming assays (Figure 1). In particular, long-read sequencing (where reads are on the order of kilobases), such as nanopore-based sequencing from Oxford Nanopore Technologies (ONT; Oxford, UK), offers several advantages compared with short-read sequencing (where read lengths may range from 100 to 250 bp).[11] Long-read sequencing better captures structural variations, particularly in repetitive regions in the human genome or where structural variations are on the order of kilobases.[12] Additionally, ONT sequencing requires lower capital investment, using benchtop sequencers, such as the MinION or PromethION.[13]

Previous work shows that RNA sequencing (RNA-seq) can be used to classify major lineages and subtypes of ALL. Walter et al[14] show that whole-transcriptome sequencing (WTS) can be used to identify 97% of risk-stratifying fusion subtypes across 279 cases of ALL. Additionally, Bařinka et al[15] show how their software, RNAseqCNV, can detect large-scale copy number variations (CNVs) in the case of B-ALL aneuploidy with 99.1% accuracy. MD-ALL integrates multiple classifiers (including RNAseqCNV) to derive genetic lesions, CNVs, and mutations for B-ALL subtyping on

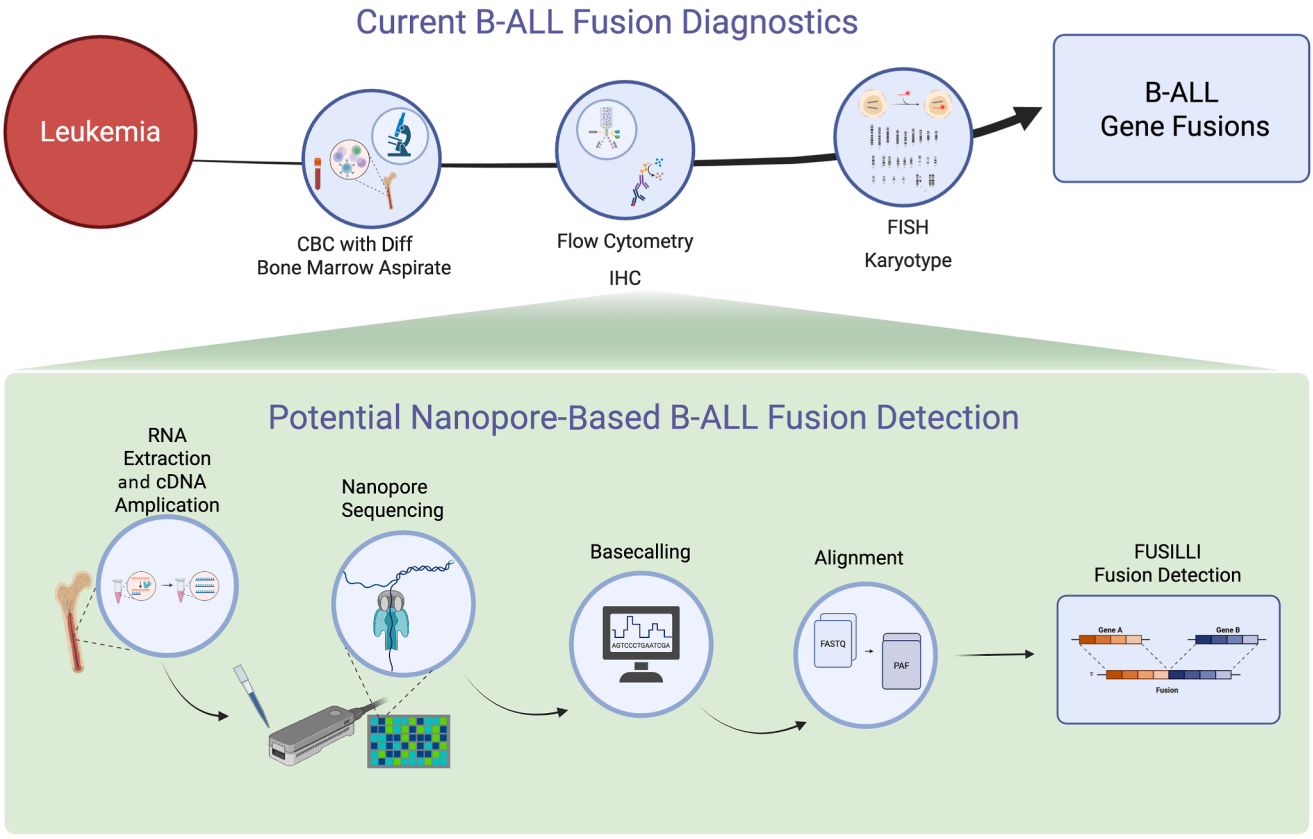

Figure 1 Comparison of conventional B-cell acute lymphoblastic leukemia (B-ALL) fusion diagnostics (**top**) and Nanopore-based fusion detection (**bottom**). Current diagnostics involve multiple tests, whereas next-generation sequencing methods, such as Oxford Nanopore Technologies whole-transcriptome sequencing (ONT-WTS), may reduce complexity and the number of different assays. FUSILLI offers a potential method for direct detection of B-ALL fusions from ONT-WTS. The image was generated using BioRender.com (Toronto, ON, Canada). CBC, complete blood cell count; Diff, differential; FISH, fluorescence *in situ* hybridization; IHC, immunohistochemistry.

a single platform.[16] Additionally, Schmidt et al[17] developed ALLSorts, a logistic regression classifier trained on B-ALL RNA-seq, to identify 18 subtypes with an overall 92% accuracy. These methods differ in computational approaches, but show the potential of using RNA-seq to determine genomic subtypes of B-ALL, including gene fusion subtypes. However, all of these methods are based on short-read sequencing, and effective computational tools are necessary to analyze ONT sequencing data to support the accurate identification of subtype-defining genomic variants.

There are several existing gene fusion detection algorithms based on long-read, WTS, including FusionSeeker, JAFFAL, and LongGF.[18–20] Notably, previous work shows LongGF outperforms other general-purpose fusion callers in terms of sensitivity at varying levels of read depth.[21] On simulated long-read RNA-seq data sets, recall rates vary between 0.86 and 0.93 using LongGF. In contrast, more recent work shows FusionSeeker outperforms both JAFFAL and LongGF.[18] In simulated ONT data sets, FusionSeeker showed (on average) superior recall rates of 0.99 and a higher F1 score of 0.93, compared with both JAFFAL and LongGF. However, few studies evaluate the performance of fusion callers in the context of identifying clinically relevant B-ALL fusions.

FUSILLI (FUSions In Leukemia Long-read sequencing Investigator version 0.1.0) is a targeted approach for identifying B-ALL gene fusions based on ONT-WTS. FUSILLI was evaluated against other fusion callers based on long-read, WTS, including FusionSeeker version 1.0.1, JAFFAL version 2.3, and LongGF version 0.1.2. Additionally, read depths needed to optimize fusion detection sensitivity were assessed through *in silico* down sampling of B-ALL FASTQ files. FUSILLI outperforms other fusion callers in terms of sensitivity and overall F1 score. Using this approach, a read depth on the order of 10 million reads is needed to obtain high sensitivity.

Materials and Methods

Samples

For the low-depth cohort, RNA extraction was performed on 68 distinct B-ALL samples with known genomic subtypes [from the University of North Carolina, St Jude Children's Research Hospital (SJCRH; samples collected through SJCRH Total XV and Total XVI protocols), and the Eastern Cooperative Oncology Group—American College of Radiology Imaging Network Cancer Research Group (samples collected through protocol E1910)] from cryopreserved bone marrow and peripheral blood mononuclear cells. RNA extraction was performed using Zymo (Irvine, CA) direct-Zol, Thermo Fisher Scientific (Waltham, MA) TRIzol/chloroform, or Qiagen (Hilden, Germany) column, per manufacturers' protocols. The high-depth cohort is a subset of the low-depth cohort, consisting of 51 B-ALL samples. Samples' genomic subtypes were determined through traditional cytogenetic karyotyping and fluorescence *in situ* hybridization and, for SJCRH samples, additional molecular diagnostic assays, including Illumina (San Diego, CA) DNA and RNA sequencing. Specific fusions detected from short-read RNA-seq [Illumina HiSeq 2000 and 2500 sequencers with fusion analysis performed by CICERO, FusionCatcher, and manual review; see Gu et al[22] (Supplementary Table ST1.Cohort, column fusion)] were used to supplement primary genomic subtypes in this study (see fusion column in Supplemental Tables S1 and S2 for the low- and high-depth genomic characteristics, respectively).[22] For example, Nano_Leuk_0097_HD (Ph-like) shows evidence of *SSBP2*::*PDGFRB* from the previous study.

Library Preparation and Transcriptome Sequencing

Full-length RNA-seq/cDNA library preparation was performed using ONT's PCR-cDNA Barcoding Kit (SQK-PCB109/110/112), according to the manufacturer's protocol. Briefly, RNA was reverse transcribed with Maxima H-RT (Thermo Fisher Scientific) using a [3′ PCR primer]-dT30VN primer to extend from the 3′ end (poly-A tail). Terminal transferase—mediated strand switching with a [5′ PCR primer]-rGrGrG strand-switching primer results in full-length first-strand cDNA synthesis with outer PCR primers. PCR amplification of cDNA is performed for 14 cycles using barcoded outer primers. Barcoded cDNA samples are pooled equimolar, followed by sequencing adapter attachment using ONT's Rapid Adapter chemistry. In the low-depth cohort, biological and technical replicates were run for some samples, resulting in 119 cDNA preparations across the 68 samples. For the low-depth cohort, up to 12 samples were multiplexed per ONT's MIN106D flow cell (R9.4.1) and sequenced for up to 48 hours on the MinION or GridION. A subset of samples were run individually on Flongle (FLG001). Reads were base called and demultiplexed using Guppy (high-accuracy mode). The high-depth cohort was sequenced similarly, but five samples were multiplexed per ONT's PromethION flow cell (R9.4.1) on PromethION 2 Solo.

Data Preprocessing

FASTQs generated from ONT-WTS were first aligned to human reference genome GRCh38.p14 (assembly accession GCF_000001405.40, *https://www.ncbi.nlm.nih.gov/datasets/genome/GCF_000001405.40*, last accessed February 23, 2024), to generate alignment files for LongGF and FUSILLI (Figure 2). FUSILLI requires Pairwise mApping Format (PAF) files, whereas FusionSeeker and LongGF require BAM files, and JAFFAL requires FASTQ files as input. PAF and binary alignment map (BAM) files were generated using "minimap2 -cx splice" and "minimap2 -ax splice", respectively. Additionally, BAM files were sorted by read identifier for LongGF. For FusionSeeker, FASTQ files were aligned using the hg38 genomic reference (*https://*

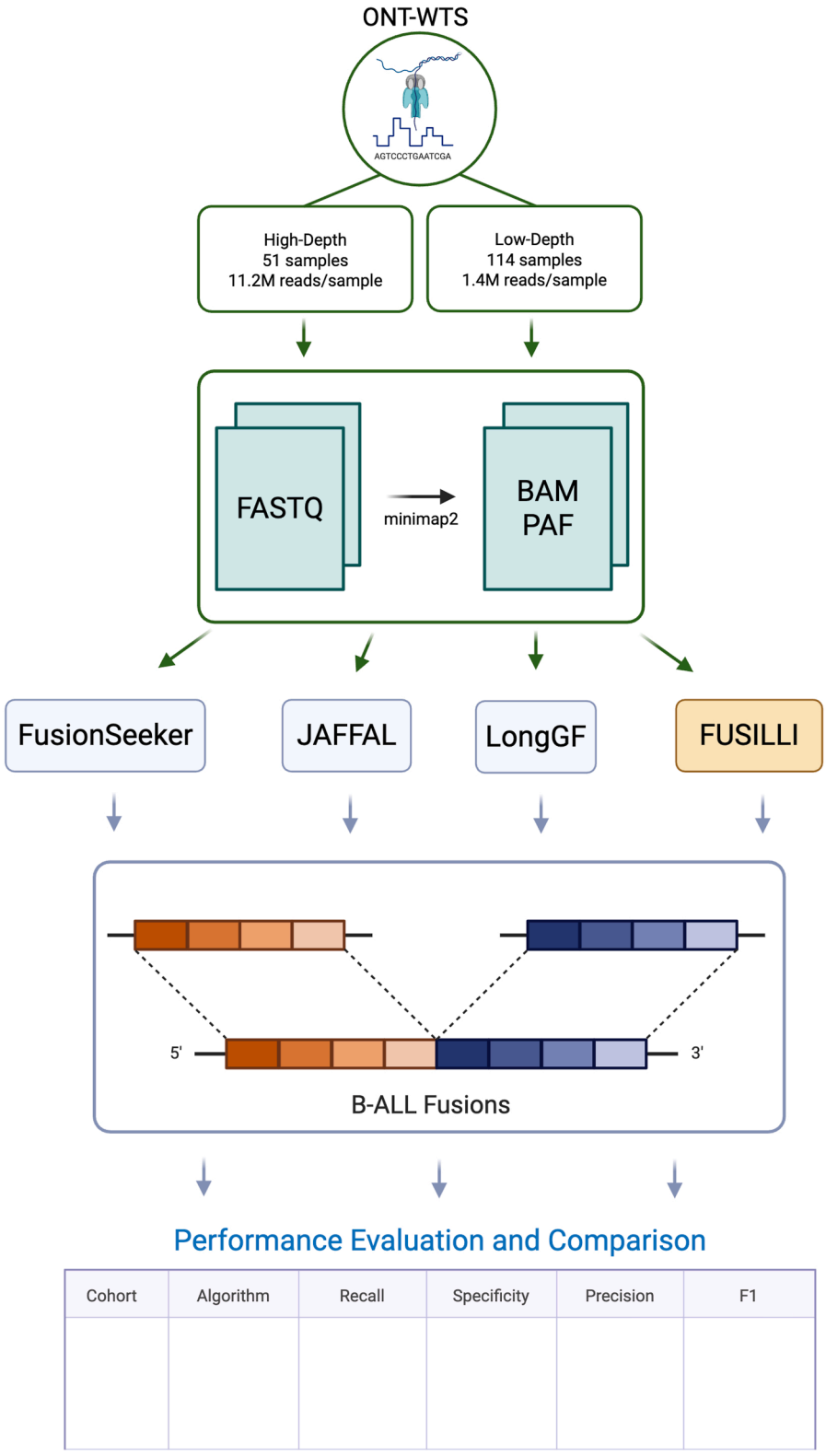

Figure 2 Overview of methods for fusion caller performance evaluation. For the high- and low-depth cohorts, Oxford Nanopore Technologies whole-transcriptome sequencing produces sequencing data in the form of FASTQ files, which are aligned using minimap2, using a reference genome, where needed. The resulting alignment files (in PAF/BAM format) are used as input for fusion callers. Results are aggregated, and performance metrics are calculated for each cohort and algorithm. The image was generated using BioRender.com (Toronto, ON, Canada). B-ALL, B-cell acute lymphoblastic leukemia; M, million.

hgdownload.gi.ucsc.edu/goldenPath/hg38/bigZips/hg38.fa.gz, last accessed December 11, 2025), and subsequent BAM files were sorted by coordinate as required.

Fusion Detection Algorithms

Broadly, each fusion caller finds candidate fusions by looking for alignments to disparate genes of interest. Then, various filtering criteria are applied to filter reads supporting fusions. Each caller is explained in more detail below.

FusionSeeker

FusionSeeker takes input BAM files along with a gene transfer format (GTF) file (hg38 reference genome and ENSEMBL version 104 GTF, provided in FusionSeeker's GitHub).[18] It scans alignment files for candidate fusions, which are clustered using density-based spatial clustering of applications with noise. Candidate fusions are further filtered on the basis of the number of supporting reads. FusionSeeker outputs confidently detected fusions along with fused transcript consensus sequences derived from partial order alignment algorithm. FusionSeeker was installed per GitHub instructions (*https://github.com/Maggi-Chen/FusionSeeker*, last accessed December 8, 2025). The nanopore variant of FusionSeeker was run in conjunction with the default GTF, as noted above.

JAFFAL

JAFFAL detects gene fusions in several stages.[19] First, it finds candidate gene fusions by alignment to a transcriptomic reference. Then, it filters candidate gene fusions by subsequent alignment to a genomic reference. Resulting gene fusion breakpoints are refined by anchoring breakpoints to exon boundaries with the idea that fused transcripts typically result from breakpoints occurring at the starts and ends of exons. JAFFAL outputs gene fusions grouped by confidence, determined by the number of supporting reads and breakpoint proximity to exon boundaries. JAFFAL was run using apptainer and the docker image at docker://davidsongroup/jaffa:latest (*https://github.com/Oshlack/JAFFA/wiki/HowToSetUpJAFFA*, last accessed December 3, 2025) for long reads. Because JAFFAL uses minimap2 to perform alignment, the only required input were FASTQ files. Additionally, a local version of the tools.groovy file specifying reformat="/JAFFA/tools/bin/reformat qin=33" was used to also analyze reads with lower base qualities (as documented at *https://github.com/Oshlack/JAFFA/issues/99*, last accessed December 10, 2025). Gene fusions from all confidence levels were considered for performance evaluation.

LongGF

LongGF detects gene fusions by first mapping RNA-seq reads to a reference and then identifies candidate gene fusion read pairs by comparison against a user-supplied GTF.[20] It filters supporting reads using various read criteria, including a binning strategy to provide an estimated breakpoint for each reported gene fusion. LongGF requires a BAM file as input along with a GTF file. LongGF was installed per GitHub instructions (*https://github.com/WGLab/LongGF*, last accessed April 3, 2024). Because LongGF is tailored toward reference data sets in GENCODE (GENome annotation based on the ENCyclopedia Of DNA Elements project) format, resulting BAM and GTF files were reformatted to correspond to GENCODE format. Additionally, LongGF was adapted (as detailed at *https://github.com/WGLab/LongGF/issues/19*, last accessed April 3, 2024) to enable fusion detection in GTF files derived from RefSeq (National Center for Biotechnology Information's Reference Sequence database). See Supplemental Table S3 for fusion calling parameters used for LongGF. Ultimately, LongGF outputs detected gene fusions along with supporting read counts and estimated breakpoints.

FUSILLI

FUSILLI requires a PAF file (aligned to a genomic reference) for each sample to cross reference with a browser extensible data (BED) file with relevant B-ALL gene chromosome, start and end positions (Supplemental Table S4). See Figure 3 for an overview of FUSILLI's process, which consists of four stages: i) Following alignment, FUSILLI looks for reads covering genomic regions specified in the B-ALL BED file by at least 50 bp (Figure 3A). Relevant genes were determined as specified in the approach detailed in *B-ALL Gene Fusion Master*. Then, using those reads, FUSILLI determines which reads span two disparate genes of interest, generating a list of reads supporting candidate B-ALL fusions. ii) FUSILLI filters candidate fusions using various filtering criteria. As shown in Figure 3B, i) genes on the read must be $\leq$30 bp apart. If the genes on the read overlap, the overlapping distance must be $\leq$50 bp. ii) Additionally, in the case of overlapping genes on a read, the overlapping distance must be $<$40% of the alignment length of gene 1 and $<$40% of the alignment length of gene 2. iii) Finally, the genomic positions of breakpoints of each gene must reside within the respective gene window, defined as the gene's start minus 10 bp through the gene's end plus 10 bp. For instance, the breakpoint location corresponding to gene 1 of a candidate fusion must be within gene 1's start and end (with 10 bp of buffer on each side). iii) As shown in Figure 3C, the candidate fusions are further filtered on the basis of the B-ALL gene fusion master (the candidate fusion must represent a gene pair from the list of B-ALL fusions previously identified). See Supplemental Table S5[23] and *B-ALL Gene Fusion Master* for details on generating the list of B-ALL gene fusions. iv) Finally, as seen in Figure 3D, only fusions with at least two unique supporting reads are output from FUSILLI by default. Supplemental Figure S1 shows most false-positive fusions

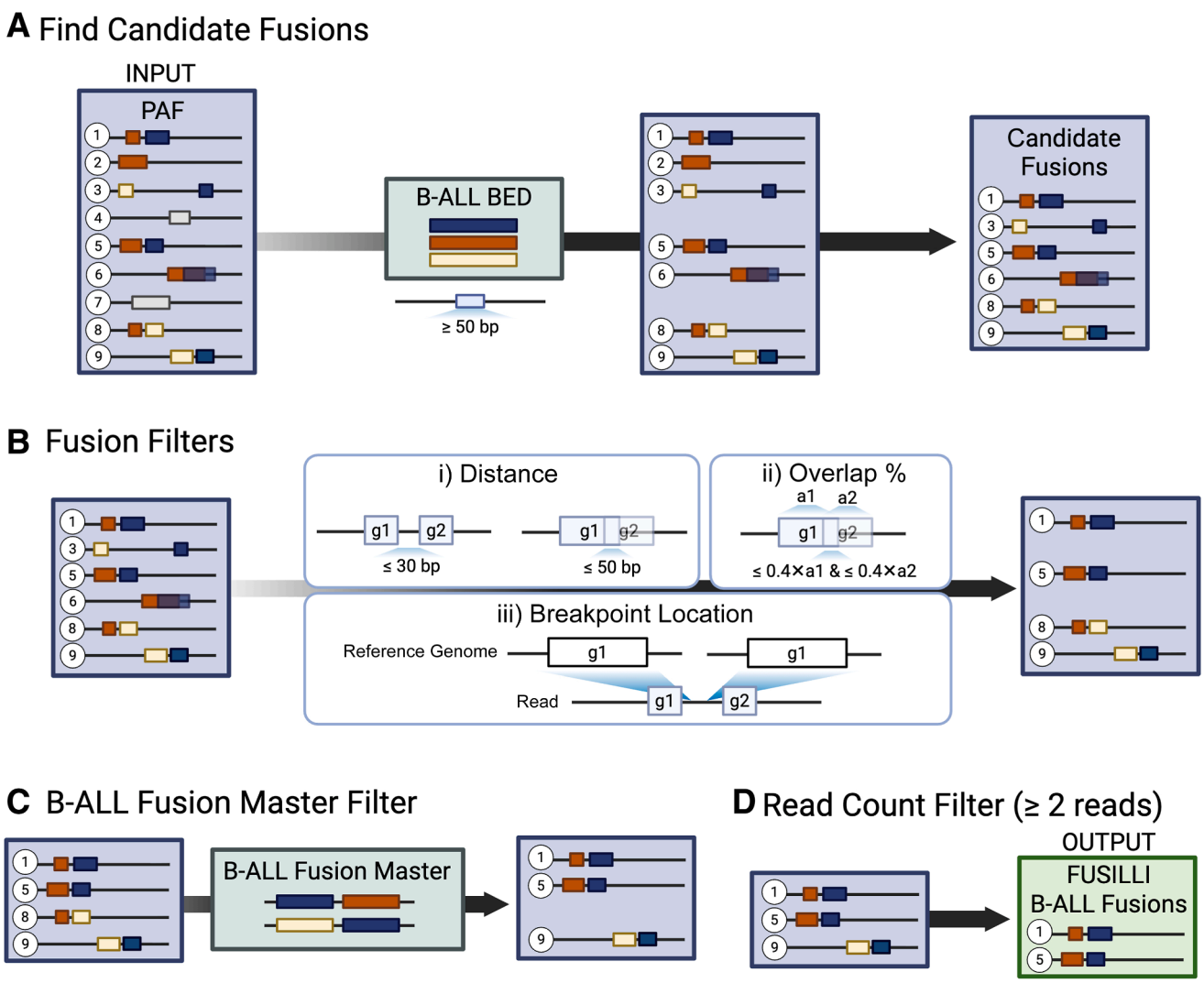

Figure 3 An overview of FUSILLI. **A:** Alignment files in PAF format are input to FUSILLI. By cross referencing a B-cell acute lymphoblastic leukemia (B-ALL) BED file with relevant B-ALL genes' genomic coordinates, reads are identified that align to B-ALL genes. B-ALL genes are shown in blue, orange, and yellow. Reads containing gray genes (non—B-ALL genes) and reads aligning to only a single B-ALL gene in the PAF file are filtered. Candidate fusions are identified from reads that align to two distinct B-ALL genes. As a result, reads 2, 4, and 7 are removed. **B:** The candidate fusions are further filtered on the basis of gene distance, overlapping percentage, and breakpoint locations. Filter i) shows candidate fusions are removed if genes (represented by g1 and g2) are >30 bp apart on the read. Read 3 has genes further than 30 bp apart, so it is removed. If they overlap, they must not overlap by >50 bp. Read 6 has genes overlapping >50 bp, so it is also removed. In ii), if the genes are overlapping on the read, they must not overlap by >40% of the alignment length (a1) corresponding to gene 1 and likewise for gene 2 (a2; representing the alignment length of gene 2). In filter iii), the breakpoint genomic locations must be within gene windows that are the start and end of each gene ± 10 bp, respectively. **C:** Only candidate fusions that represent a gene pair on the B-ALL fusion master are kept. Here, read 8 contains a gene pair absent from the B-ALL fusion master, so it is removed. **D:** Finally, only candidate fusions with at least two unique supporting reads are output as FUSILLI's detected B-ALL fusions. The yellow and blue fusion only has one supporting read (represented by read 9), so it is removed. The orange and blue fusion has two unique supporting reads, so it would be the only fusion reported in this example. The image was generated using BioRender.com (Toronto, ON, Canada).

have one supporting read compared with most true-positive fusions, which have at least two supporting reads. False positives with one supporting read are often technical chimeric reads resulting from (post-PCR) ligation or sequencing. These are rare events and unlikely to result in consistent, rational cDNA breakpoints.[24,25] FUSILLI's above filtering criteria were determined through analyses of candidate fusion-supporting reads. See Supplemental Table S3 and *https://github.com/jwanglab/fusilli/blob/main/fusilli.py* (last accessed December 4, 2025) for more details on specific filtering parameters used.

Fusion Detection Evaluation

B-ALL Gene Fusion Master

To determine the scope of relevant B-ALL fusions, a B-ALL gene master list was generated from previous work detailing the comprehensive landscape of ALL genomic subtypes (see

Table 1 High-Depth Cohort Sequencing Characteristics

Genomic subtype category	Genomic subtype	Samples, *n*	Reads/sample, mean	Read lengths/sample, mean	N50, mean	Reads aligned/sample, mean	% Reads aligned/sample, mean
Ploidy	High hyperdiploid	13	6,854,212	543	815	3,507,100	53.11
Ploidy	Low hypodiploid	7	11,669,028	397	491	1,479,271	29.84
Ploidy	Near haploid	5	12,270,344	432	532	1,631,541	32.79
Fusion	*ETV6*::*RUNX1*	12	10,867,859	584	901	5,804,838	54.42
Fusion	*BCR*::*ABL1*	8	16,956,542	444	650	4,750,014	30.27
Fusion	Ph-like	3	16,031,361	554	850	5,911,279	46.50
Fusion	*MEF2D*r	2	9,871,346	298	418	1,080,247	14.62
Fusion	*TCF3*::*PBX1*	1	4,987,963	462	698	2,442,779	48.97
	Overall	51	11,196,687	495	721	3,805,886	42.67

Ph, Philadelphia chromosome.

Brady et al[23]). First, single partner genes were parsed from B-ALL gene fusions detected from RNA-seq or whole-genome sequencing. The number of samples associated with a given gene was calculated from the number of samples containing the gene within detected fusions. To mitigate the proliferation of fusion singletons, only genes that occurred in at least two distinct samples were included in the FUSILLI BED file previously described. Fusion genes were determined from the list of unique partner genes' associated gene partners in detected fusions. Overall, there are 74 unique fusions across 65 partner genes (fusions involving *DUX4*::*IGV* were interpreted as *IGH*::*DUX4* rearrangements). See Supplemental Table S4 for the BED file of B-ALL genes and Supplemental Table S5 for the list of relevant B-ALL fusions.

Fusion Performance Evaluations

For each fusion caller, the sample's dominant fusion was determined by the detected B-ALL gene fusion with the most number of supporting reads, in cases where multiple B-ALL gene fusions were detected (see the top_detected_fusion in the summary of results for FusionSeeker, JAFFAL, LongGF, and FUSILLI in Supplemental Tables S6 to S9). The dominant fusion was compared against the sample's true fusion to determine sample class (true/false positive or negative, see columns fusion and sample_class in Supplemental Tables S6 to S9). There were 27 of 51 and 79 of 119 samples with known B-ALL fusions in the high- and low-depth cohorts, respectively. The low-depth cohort contained 119 different sequencing runs across 68 distinct B-ALL samples. However, the low-depth evaluations were conducted using the 119 sequencing runs as the set of classifications.

Performance evaluations were calculated per standard formulas for sensitivity, specificity, precision, and F1 score. True positives represent concordance between the dominant detected fusion and the sample's true fusion subtype. True negatives represent samples with no fusion and no relevant B-ALL fusion detected. False negatives represent samples with a true B-ALL fusion, but there was no fusion detected at all. False positives represent samples where a B-ALL fusion was detected but did not

Table 2 Low-Depth Cohort Sequencing Characteristics

Genomic subtype category	Genomic subtype	Samples, *n*	Reads/sample, mean	Read lengths/sample, mean	N50, mean	Reads aligned/sample, mean	% Reads aligned/sample, mean
Ploidy	High hyperdiploid	17	2,066,933	433	609	1,199,886	59.40
Ploidy	Near haploid	12	2,973,052	447	590	1,910,934	53.85
Ploidy	Low hypodiploid	11	251,309	540	649	157,884	57.41
Fusion	*ETV6*::*RUNX1*	19	2,315,836	466	670	1,236,551	57.61
Fusion	*BCR*::*ABL1*	16	877,212	506	699	473,317	57.41
Fusion	*DUX4*r	12	218,077	349	389	78,800	40.58
Fusion	*ZNF384*r	10	266,152	708	937	214,374	71.73
Fusion	Ph-like	8	706,335	391	500	479,434	59.97
Fusion	*TCF3*::*PBX1*	6	1,393,107	810	1076	1,080,399	78.23
Fusion	Ph-like (non-*CRLF2*)	4	2,722,282	787	974	2,075,743	81.58
Fusion	*MEF2D*r	3	350,227	531	704	231,595	62.97
Fusion	*KMT2A*r	1	197,423	525	779	162,275	82.20
	Overall	119	1,370,085	505	670	829,418	59.26

Ph, Philadelphia chromosome.

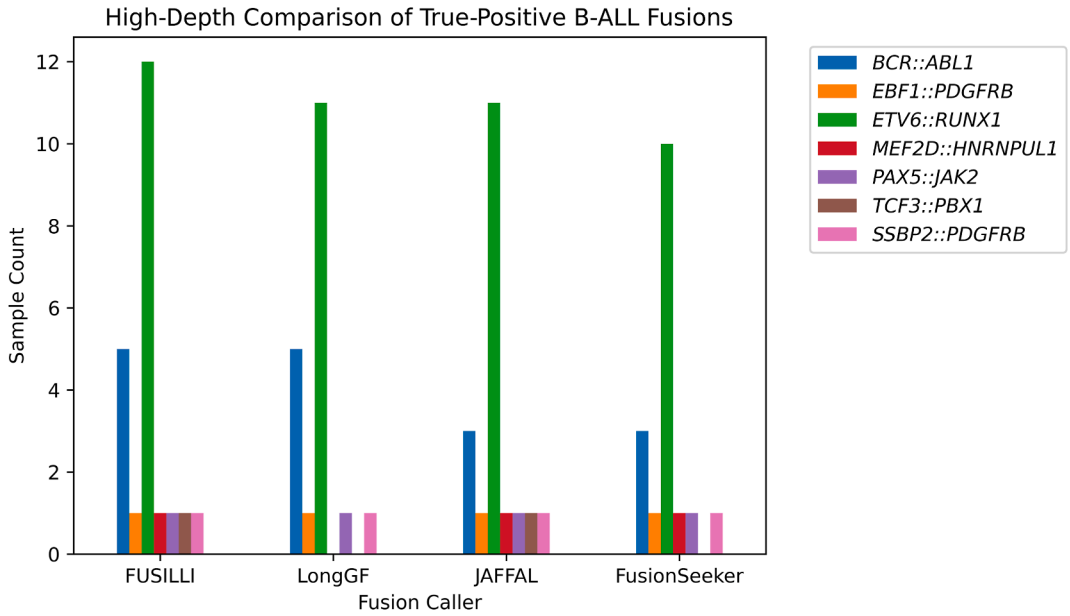

Figure 4 Comparisons of true-positive fusions detected between different fusion callers for the high-depth cohort. Each group on the *x* axis represents fusions detected from a given fusion caller. Colors indicate the detected fusion. FUSILLI outperforms other fusion callers for most B-cell acute lymphoblastic leukemia (B-ALL) fusion subtypes.

correspond with the sample's true fusion or the sample did not have a B-ALL fusion. Although the dominant fusion for each sample was used to determine sample class, there are likely secondary fusions that may represent *bona fide* fusions. Therefore, all fusions detected are documented in the detected fusion column in Supplemental Tables S6 to S9 along with the fusion_class (true positive or false positive). Performance metrics were considered on a per-fusion level, but there were not enough cases per fusion to represent meaningful metrics. *PAX5*::*ZCCHC7* was excluded from performance evaluation for reasons discussed below (see *FUSILLI Detects* PAX5::ZCCHC7 *Secondary Alterations across a Mix of B-ALL Genomic Subtypes*).

Sequencing Metrics

Each sample's number of reads, mean read length, N50, and number of reads aligned were generated using NanoStat version 1.6.0 (for FASTQ) and cramino version 0.16.0 (for BAM files).[26] Sequencing metrics, as shown in Tables 1 and 2, were calculated in Python version 3.12.9 (*https://www.python.org*) and stratified by genomic subtype.

Read Depth and Read Length Studies

In silico down sampling was conducted using seqtk version 1.4 (*https://github.com/lh3/seqtk*) Reads were randomly subsampled from the high-depth cohort's FASTQ files using "seqtk sample -s". The number of reads to subsample was determined as a percentage (ranging from 10% to 90%) of each sample's number of total reads in a given FASTQ file. Additionally, each subsampling was repeated 10 times, generating 90 additional FASTQ files for each of the 51 samples in the high-depth cohort. The resulting FASTQ files were aligned and analyzed for fusions using FUSILLI, and corresponding fusion performance metrics were calculated as described in *Fusion Detection Evaluation*. Read lengths stratified by fusion subtype were generated by aggregating the read summary FUSILLI outputs (–report option) and plotting the distributions of supporting read lengths (filtered to reads passing filtering criteria) for true-positive fusions.

Results

FUSILLI Outperforms LongGF Detection of Relevant Fusion Subtypes in B-ALL Samples Sequenced at High Depth

For the high-depth cohort, FUSILLI showed the greatest sensitivity (0.81) (Figure 4 and Table 3) compared with other fusion callers, resulting in a superior F1 score (0.86). The average read length was 495 bp, with 11.2 million reads per sample (Table 1) across several gene fusion subtypes (see Supplemental Table S2 for true fusion subtypes). Between FusionSeeker, JAFFAL and LongGF, LongGF performed the best in terms of F1 score (0.81) and detected 70% of B-ALL fusions. JAFFAL recalled more fusions than LongGF (sensitivity of 0.76), but specificity was worse (0.81), resulting in a lower F1 score. See Supplemental Tables S6 to S9 for the B-ALL fusions detected and sample classifications across all algorithms. As shown in Table 4 and compared with LongGF, FUSILLI detected fusions *TCF3*::*PBX1*, *ETV6*::*RUNX1*,

Table 3 High-Depth Fusion Caller Comparison

Algorithm	Sensitivity (recall)	Specificity	Precision	F1
FusionSeeker	0.63	**0.96**	0.94	0.76
JAFFAL	0.76	0.81	0.79	0.78
LongGF	0.70	**0.96**	**0.95**	0.81
FUSILLI	**0.81**	0.92	0.92	**0.86**

Numbers in bold delineate the highest scoring metric with respect to each column.

and *MEF2D*::*HNRNPUL1*, but was unable to detect 5 of 27 samples with known B-ALL gene fusions. FUSILLI could not detect *BCR*::*ABL1* in three samples, *MEF2D*::*BCL9* in one sample, and a *CRLF2*r in a near-haploid sample. Further investigation showed there was one supporting read each for the *MEF2D*::*BCL9* sample (Nano_Leuk_0231_HD) and two *BCR*::*ABL1* samples (Nano_Leuk_0232_HD and Nano_Leuk_0233_HD), which did not satisfy FUSILLI's threshold of two supporting reads.

FUSILLI Is Computationally Efficient Compared with FusionSeeker and LongGF

All methods were tested using an Intel (Santa Clara, CA) Xeon E5-2680 version 3 workstation running Red Hat Enterprise Linux 9 with 48 logical central processing units (CPUs) and 361 GB of RAM. In the high-depth cohort, following alignment to a genomic reference, FUSILLI ran (on average) 1 minute 45 seconds (wall clock time) per sample and used 2.13 GB of RAM. In comparison, FusionSeeker, JAFFAL, and LongGF took between 10 and 97 minutes and used 8 to 46 GB of RAM per sample (on average) (Table 5). JAFFAL performs alignment from input FASTQ files, so it was difficult to evaluate its fusion-specific performance alone. Compared with FusionSeeker and LongGF, FUSILLI was fastest and required fewer computing resources. By default, FUSILLI focuses on a limited set of 65 genes specific to B-ALL, whereas other general-purpose fusions callers consider genes across the entire transcriptome.

Table 4 False Negatives Reported by LongGF and FUSILLI

Sample	Gene fusion subtype	LongGF detected?	FUSILLI detected?
Nano_Leuk_0051_HD	*TCF3*::*PBX1*	N	Y
Nano_Leuk_0054_HD	*ETV6*::*RUNX1*	N	Y
Nano_Leuk_0226_HD	Near haploid (with *CRLF2*r)	N	N
Nano_Leuk_0230_HD	*MEF2D*::*HNRNPUL1*	N	Y
Nano_Leuk_0231_HD	*MEF2D*::*BCL9*	N	N
Nano_Leuk_0232_HD	*BCR*::*ABL1*	N	N
Nano_Leuk_0233_HD	*BCR*::*ABL1*	N	N
Nano_Leuk_0235_HD	*BCR*::*ABL1*	N	N

N, no; Y, yes.

FUSILLI Detects Fusions across a Wide Range of Read Lengths

Figure 5 shows a wide range of mean read length per sample and number of supporting reads for FUSILLI fusions. For example, *BCR*::*ABL*1 fusions were correctly detected across several samples, with at least two supporting reads and with mean read lengths per sample ranging from 249 to 796 bp. Additionally, *ETV6*::*RUNX1* fusions were correctly detected in samples with mean read lengths ranging from 358 to 844 bp and number of supporting reads ranging from 6 to 384 reads. In samples where gene fusions were missed, as mentioned above [Nano_Leuk_0231_HD (*MEF2D*::*BCL9*), Nano_Leuk_0232_HD (*BCR*::*ABL1*), and Nano_Leuk_0233_HD (*BCR*::*ABL1*)], mean read lengths were on the lower end of the spectrum, ranging from 215 to 246 bp. Although one supporting read was found for the respective fusions, they did not satisfy FUSILLI's default minimum threshold of two supporting reads. Further inspection of these samples showed poor alignment rates between 4% and 8% (Supplemental Table S10). Although average blast percentages were high (80%), RNA quality may have been low, leading to shorter read lengths, poor alignment rates, and fusion detection.

FUSILLI Detects *PAX5*::*ZCCHC7* Secondary Alterations across a Mix of B-ALL Genomic Subtypes

PAX5::*ZCCHC7* was detected across 10 samples (Figure 6). This included four *ETV6*::*RUNX1*, two high hyperdiploid, three Ph-like, and one *BCR*::*ABL1* sample(s). *PAX5*::*ZCCHC7* is a secondary fusion, which has previously been reported to co-occur with other subtype-defining alterations, such at *ETV6*::*RUNX1*, *IGH*::*DUX4*, and Ph-like subtypes.[22,27,28] Another recent study showed *PAX5*::*ZCCHC7* occurs in a wide range of other B-ALL subtypes, including *TCF3*::*PBX1* and hyperdiploid samples.[29] Interestingly, for sample Nano_Leuk_0233_HD, FUSILLI detected *PAX5*::*ZCCHC7* (Figure 6), but did not detect the primary *BCR*::*ABL1* subtype with sufficient read support. Given *PAX5*::*ZCCHC7*'s known prevalence in B-ALL subtypes, *PAX5*::*ZCCHC7* was white-listed as a secondary alteration, thereby excluding *PAX5*::*ZCCHC7* from performance evaluations.

The True Genomic Subtype Often Correlates with the Dominant Fusion Detected by FUSILLI, with Few Cases Requiring Manual Review

FUSILLI detected the leukemic-driving fusion as the most dominant fusion in 21 of 22 samples classified as true positive. Only Nano_Leuk_0098_HD (Ph-like) showed *PAX5*::*ZCCHC7* as the dominant fusion, which is comparable in read support to *EBF1*::*PDGFRB*, which is a Ph-like-associated fusion (17 and 16 reads, respectively). For other cases, the number of supporting reads for supplemental fusions paled in comparison to that of the true fusion

Table 5 Comparison of Computational Efficiency across Fusion Callers (High-Depth Cohort)

Algorithm	Average real time	Average CPU time	Average RAM used, GB
FusionSeeker	50 Minutes 26 seconds	85 Minutes 53 seconds	30.01
JAFFAL*	96 Minutes 7 seconds	175 Minutes 13 seconds	45.31
LongGF	10 Minutes 22 seconds	9 Minutes 54 seconds	8.88
FUSILLI	**1 Minute 45 seconds**	**53 Seconds**	**2.13**
minimap2*	157 Minutes 55 seconds	752 Minutes 44 seconds	31.75

Numbers in bold delineate the most efficient metric with respect to each column.

*JAFFAL performs alignment to a transcriptomic reference from FASTQ files by default. All other algorithms were evaluated on fusion detection after alignment using minimap2 (minimap2 -t 8) to a genomic reference, included as the last row for comparison.

subtype. Nano_Leuk_0065_HD (*ETV6*::*RUNX1*, 384 reads) showed evidence of *SSBP2*::*PDGFRB* (2 reads), whereas Nano_Leuk_0067_HD (*ETV6*::*RUNX1*, 108 reads) showed evidence of *ETV6*::*EBF1* (5 reads) (Figure 6). Manual review of these two fusions in these samples would likely identify *ETV6*::*RUNX1* as the relevant fusion detected. See Supplemental Tables S9 and S11 for FUSILLI results and detailed fusion report output, respectively.

Further Investigation of Select Cases Shows Discrepancies between True Genomic Subtype and Detected Fusions

One high hyperdiploid and two Ph-like samples (Nano_Leuk_0068_HD, and Nano_Leuk_0097_HD and Nano_Leuk_0098_HD, respectively) showed evidence of *ETV6*::*RUNX1*. Realizing *ETV6*::*RUNX1* was a distinct subtype, read accuracies and breakpoint locations were compared between true- and false-positive *ETV6*::*RUNX1* cases to determine whether the observations in the false-positive cases were warranted. No discernible differences were observed between true- and false-positive cases (Supplemental Figures S2 and S3). Notably, the false-positive cases exhibited an average of 12 supporting reads, compared with 62 supporting reads in the true-positive cases for *ETV6*::*RUNX1*, which may suggest sample contamination after PCR amplification (Supplemental Table S12). Additionally, *ETV6*::*RUNX1* was not found in these cases, per SJCRH and Gu et al.[22] In contrast, the true-positive samples FUSILLI detected were

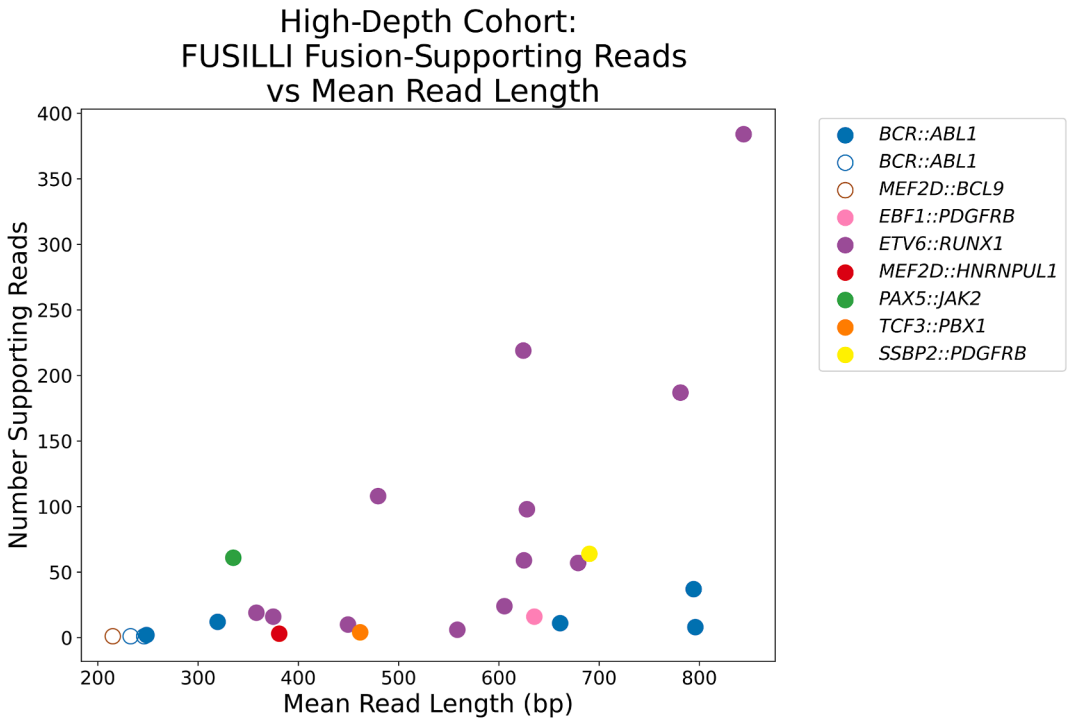

Figure 5 Number of supporting reads versus mean read lengths for fusions [limited to those that correspond to known B-cell acute lymphoblastic leukemia (B-ALL) gene fusions] detected using FUSILLI in the high-depth cohort, regardless of read support. The *x* axis represents the mean read length determined from a sample's FASTQ file. Each data point represents a B-ALL relevant fusion detected for a given sample. Filled circles represent cases where the detected fusion coincides with the true B-ALL gene fusion and there are at least two supporting reads. Empty circles represent similar concordance, but there is only one supporting read. Colors correspond to the detected fusion type. Note, only fusions with at least two supporting reads are considered a detected fusion when performing fusion detection evaluation for FUSILLI.

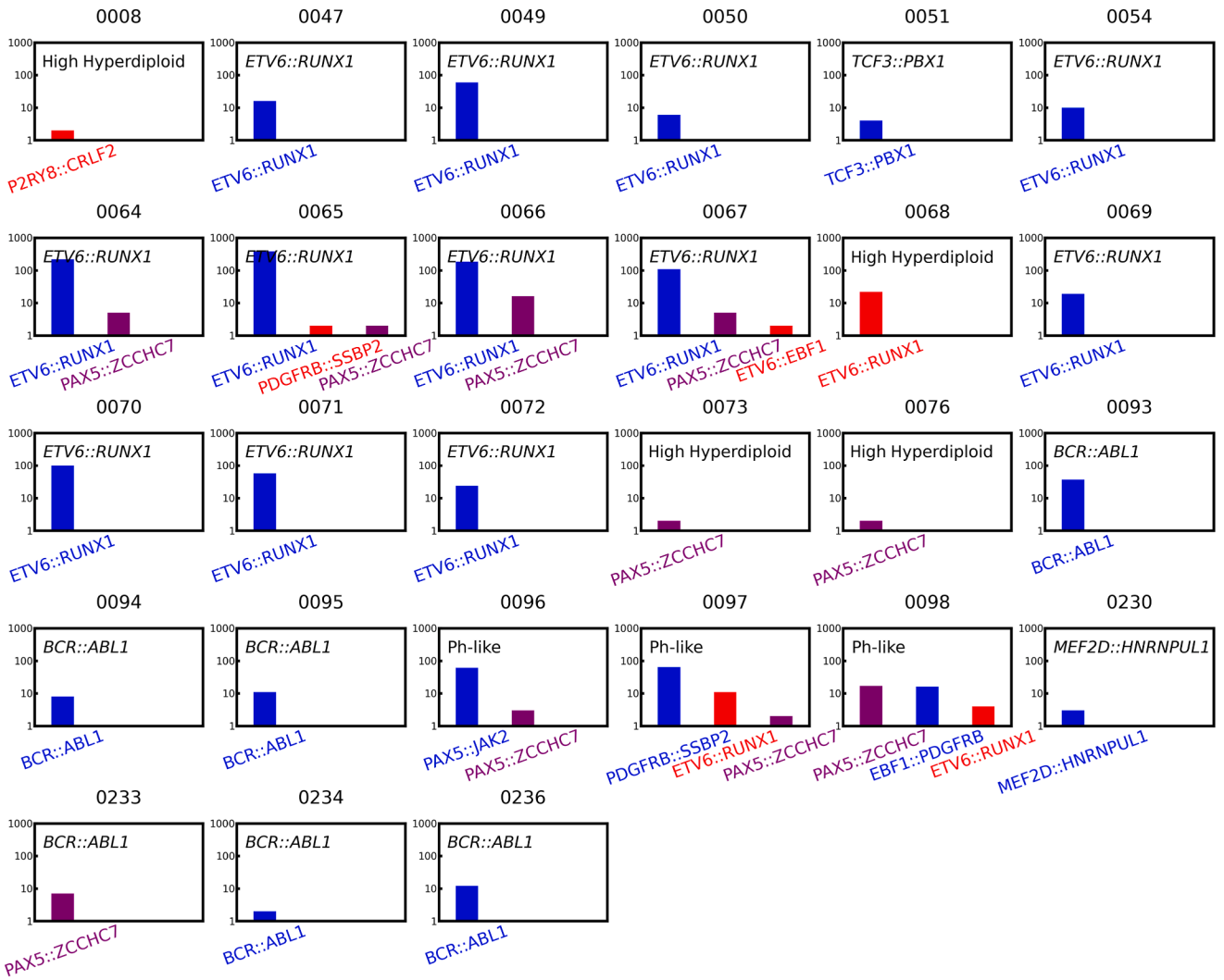

Figure 6 Distribution of all FUSILLI fusions detected per sample. Numbers in the title of each plot represent the XXXX sample number as in Nano_Leuk_XXXX_HD. The number of supporting reads are shown on the *y* axis. Blue denotes true-positive fusions (where FUSILLI fusions match previously reported fusions). True genomic subtypes are labeled for each sample and correspond to the dominant fusions in 21 of 23 samples that have B-cell acute lymphoblastic leukemia fusion subtypes. Red bars denote FUSILLI fusions that were not available in the set of previously reported fusions. *PAX5*::*ZCCHC7* fusions were excluded from performance evaluations (because of observations discussed in *Results*) and are shown here in purple. Ph, Philadelphia chromosome.

consistent with the results from additional cytogenetics and sequencing modalities from SJCRH, including fluorescence *in situ* hybridization and Illumina DNA and RNA sequencing, where available (see Supplemental Table S2 for corresponding SJCRH sample identifiers). Concordant fusions found by long-read DNA sequencing in a subset of cases provided additional support.[30] Further investigation of these cases and future analysis of a larger cohort sequenced by collaborators are needed to assess *ETV6*::*RUNX1* specificity in FUSILLI to confirm that the false positives in the present cohort were likely a result of contamination.

One hyperdiploid sample (Nano_Leuk_0008_HD) was classified as false positive, showing evidence of *P2RY8*::*CRLF2*. *P2RY8*::*CRLF2* (where both genes were located in the pseudoautosomal regions of the short arms of chromosomes X and Y) commonly arises from a deletion resulting in the juxtaposition of the promoter of *P2RY8* to the coding portion of *CRLF2*.[31,32] Previous studies show *CRLF2* rearrangements can co-occur with hyperdiploidy.[31–33] For Nano_Leuk_0008_HD, there were two supporting reads with appropriate separation between the gene alignments. Breakpoint patterns exhibit some consistency in breakpoint positions and proximity to

Table 6 Low-Depth Fusion Caller Comparison

Algorithm	Sensitivity (recall)	Specificity	Precision	F1
FusionSeeker	0.09	**1.00**	**1.00**	0.16
JAFFAL	0.23	0.95	0.90	0.36
LongGF	0.16	0.97	0.93	0.27
FUSILLI	**0.27**	0.95	0.92	**0.42**

Numbers in bold delineate the highest scoring metric with respect to each column.

exon boundaries (between 1 and 10 bp) (Supplemental Table S13). Comparison to Nano_Leuk_0238_LD (a high hyperdiploid case in the low-depth cohort) revealed similar breakpoint positions (specifically, chromosome X:1212639 for *CRLF2* and chromosome X:1536919 for *P2RY8*), although Nano_Leuk_0238_LD had 10 supporting reads.

FUSILLI Outperforms Existing Methods at Low Sequencing Depth, albeit with Limited Sensitivity

For the low-depth cohort, FUSILLI again showed the greatest sensitivity (0.27) (Table 6) compared with other fusion callers. This resulted in a superior F1 score of 0.42. In the low-depth cohort, the average read length was 505 bp, with 1.4 million reads per sample (see Table 2 and Supplemental Table S1 for true fusion metadata). Compared with the high-depth cohort, this was approximately one-tenth of the read depth (Table 1), but read lengths were comparable. Figure 7 shows the distribution of B-ALL fusion subtypes correctly detected by each algorithm. Overall, FUSILLI correctly detected 22 B-ALL fusion subtypes (of 81 samples with known genomic subtypes) (see Supplemental Tables S9 and S11 for summaries of FUSILLI's performance on the low-depth cohort). Primary genomic subtypes correctly detected from FUSILLI but not from other fusion callers included three samples of *ETV6*::*RUNX1*, one *BCR*::*ABL1*, and one Ph-like (*IGH*::*EPOR*) sample. Not surprisingly, FUSILLI showed decreased sensitivity in the low-depth cohort compared with that in the high-depth cohort (0.27 versus 0.81), as a result of decreased sequencing depth.

In Silico Read Depth Studies Show that 10 Million Reads per Sample Optimize Fusion Detection, and Supporting Read Length Varies by Fusion Type

To understand the effects of decreased sequencing depth on fusion detection performance, reads were randomly subsampled (at varying percentages from 10%, 20%, 30%, to 90%) from samples in the high-depth cohort, and FUSILLI was used to detect fusions from down-sampled files. Sensitivity, specificity, and F1 scores were subsequently calculated on the basis of fusions detected. Random subsampling, fusion detection, and evaluation were repeated 10 times for each subsampling percentage. For each iteration, the mean number of reads and minimum, maximum, and mean score of each evaluation metric were calculated. As shown in Figure 8, increasing coverage (increasing mean number of reads) shows overall gains in sensitivity and F1 score. The F1 score appears to plateau at 0.86 at 10 million reads. Although sensitivity continually increases over the entire range, specificity slightly decreases because of the detection of *P2RY8*::*CRLF2* in Nano_Leuk_0008_HD,

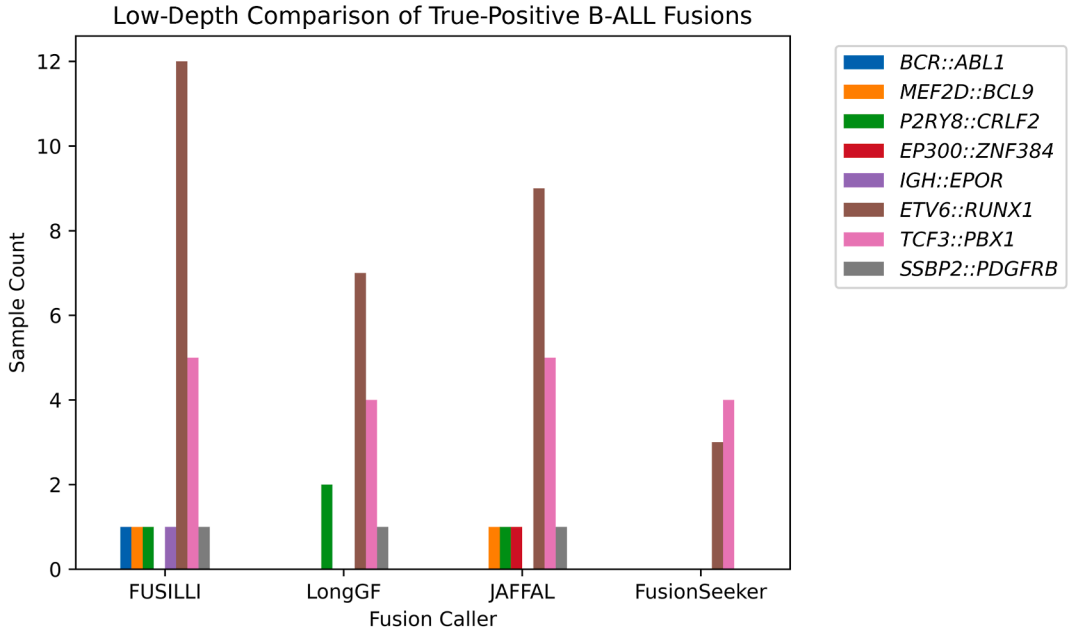

Figure 7 Comparisons of true-positive fusions detected between different fusion callers for the low-depth cohort. B-ALL, B-cell acute lymphoblastic leukemia.

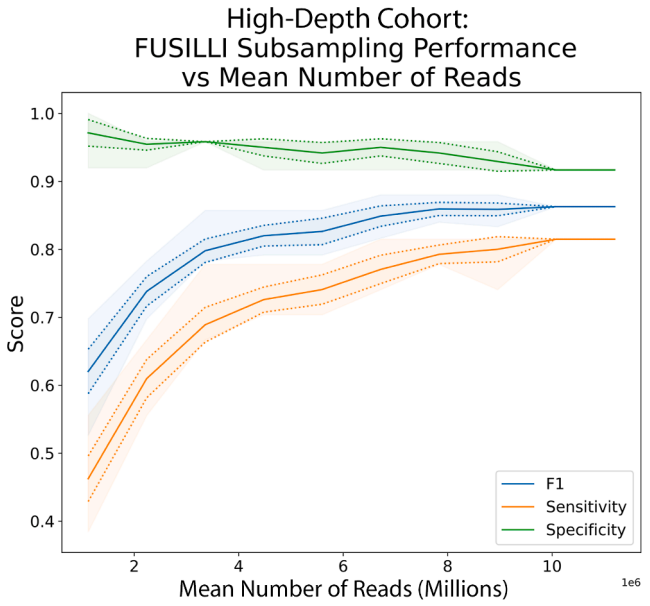

Figure 8 Effects of subsampling on sensitivity, specificity, and F1 scores from the high-depth cohort. Different subsampling percentages from the high-depth cohort were performed over 10 iterations. The *x* axis reflects the mean number of reads resulting from each subsampling percentage. **Dark lines** indicate mean score, whereas corresponding transparent boundaries are minimum and maximum scores for each metric over the 10 iterations. **Dotted lines** indicate 95% CIs. Generally, increasing sequencing depth results in improved performance.

detected at higher depths. Therefore, increasing sequencing coverage improved fusion detection performance, with most notable gains between means of one and nine million reads.

Similarly, longer read lengths likely lead to better fusion detection performance. Read length is primarily driven by RNA quality, which varies by sample handling and storage parameters. Figure 9 shows the distributions of read lengths of correctly detected fusions from the high-depth cohort. For each sample's true fusion subtype, supporting reads were isolated and distributions of supporting read lengths were plotted. Some fusion transcripts, such as *BCR*::*ABL1* (where the breakpoint may be on the order of kilobases away from the poly-A tail), may require longer read lengths to correctly detect those fusions with a supporting median read length of 2182 bp. In contrast, fusions such as *ETV6*::*RUNX1* and *TCF3*::*PBX1* reflect shorter read lengths with median read lengths of 1451 and 1183 bp, respectively. See Supplemental Table S10 for more detailed sequencing metrics per sample.

Data and Code Availability

Specimens, sequencing, and expression data used in this study were previously described.[34] FASTQ files for the high- and low-depth cohorts are available on request. FUSILLI is built in Python version 3.12.9 and available on GitHub (*https://github.com/jwanglab/fusilli/tree/main*, last accessed December 15, 2025). Directions for installation and usage are available in the README file, along with a tutorial and sample data.

Discussion

NGS methods have the potential to enhance and/or replace current diagnostic tests used to determine the genomic subtypes of B-ALL. The comprehensive diagnostic workup, which includes tests such as immunohistochemistry and fluorescence *in situ* hybridization, may take several days to complete, requiring the collaboration of various experts and

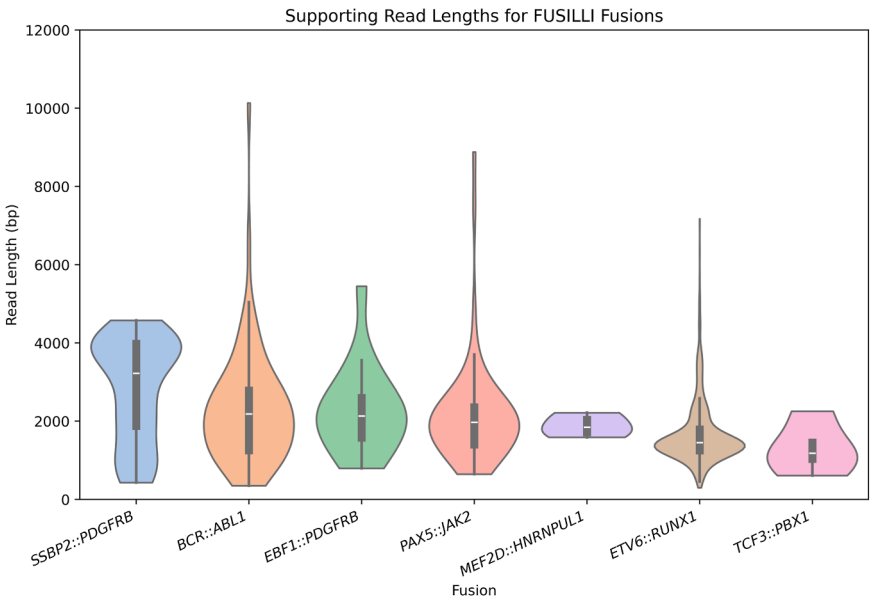

Figure 9 Violin plot of read length distributions of correctly detected fusions from the high-depth cohort, ordered from left to right by decreasing median read length.

resources. Although current NGS approaches mainly rely on short-read sequencing, ONT-WTS offers several advantages, including lower capital costs and improved detection of significant structural variations, such as aneuploidies and gene fusion transcripts. Long-read sequencing produces read lengths on the order of kilobases versus short-read sequencing with typical read lengths below 300 bp.[35] This offers better resolution, particularly in repetitive regions of the genome, where alignment of short-read sequences may be difficult. Additionally, ONT-WTS can be performed on benchtop sequencers, such as the MinION, making it highly adaptable across various resource settings. Several general-purpose, long-read fusion callers based on transcriptome sequencing exist, such as LongGF. However, few studies evaluate fusion callers in the context of identifying clinically relevant B-ALL gene fusions. Additionally, there is a lack of information on the sequencing depth required to detect B-ALL gene fusions accurately.

In the present B-ALL cohort of 51 samples sequenced at high depth (an average of 11.2 million reads per sample), FUSILLI achieved higher sensitivity and F1 score than extant methods. Compared with the next best-performing fusion caller, LongGF, FUSILLI detected additional clinically relevant fusions (*ETV6*::*RUNX1*, *TCF3*::*PBX1*, and *MEF2D*::*HNRNPUL1*) in three samples. FUSILLI could not confidently detect B-ALL gene fusions in three *BCR*::*ABL1*, one *MEF2D*::*BCL9*, and one near-haploid (harboring a *CRLF2* rearrangement) samples. For two of the three *BCR*::*ABL1* and the *MEF2D*::*BCL9* samples, FUSILLI shows one supporting read for the respective gene fusions, which does not satisfy the minimum two supporting read requirement. Sequencing at a higher depth would potentially increase sensitivity. Regarding *BCR*::*ABL1*, most ALL cases exhibit the p190 *BCR*::*ABL1* isoform, resulting in the fusion of exon 1 of *BCR* to exons 2 through 11 of *ABL1*.[36,37] Sequencing this breakpoint through reverse transcription with oligo d(T) primers is notoriously difficult because of the large distance between *ABL1* exon 2 and the poly-A tail. A canonical *BCR-ABL1* fusion starts at *ABL1* exon 2 and includes exons 2 to 11 + the 3′ untranslated region for a total of 5507 nucleotides. Therefore, in this approach, detecting *BCR*::*ABL1* fails when long reads fail to capture the distant breakpoint. Regarding the near-haploid sample, the *CRLF2* rearrangement was solicited from a previous study.[22] FUSILLI does show evidence of 14 reads supporting *P2RY8*::*CRLF2* in this sample; however, reads are ultimately filtered on the basis of read lengths >100 kbp, suggesting these are likely technical artifacts.

Further examination of supplemental fusions shows the presence of *PAX5*::*ZCCHC7* secondary alterations, which are difficult to detect through conventional clinical testing. Previous studies show *PAX5*::*ZCCHC7* co-occurs with a mix of B-ALL primary genomic subtypes, including *ETV6*::*RUNX1*, *IGH*::*DUX4*, Ph-like, *TCF3*::*PBX1*, and hyperdiploid subtypes.[22,27–29] *PAX5* encodes a critical transcription factor that regulates B-cell development.[38] Li et al[29] suggest *PAX5*::*ZCCHC7* may result in loss of *PAX5* function similar to a *PAX5* deletion, disrupting normal B-cell proliferation and development.

Other supplemental fusions require further examination. In two samples (Nano_Leuk_0065_HD and Nano_Leuk_0067_HD), which exhibit *SSBP2*::*PDGFRB* and *ETV6*::*EBF1*, the number of supporting reads range from two to five reads. These pale in comparison to the primary genomic subtype, *ETV6*::*RUNX1*, which has supporting reads ranging from 108 to 384 reads in these samples. These additional fusions could be filtered through manual review. The *P2RY8*::*CRLF2* fusion observed in the hyperdiploid sample, Nano_Leuk_0008_HD, is potentially a *bona fide* fusion, but would need further validation, such as targeted real-time quantitative PCR.

In the low-depth cohort (119 samples with an average of 1.4 million reads per sample), FUSILLI similarly outperformed the other evaluated fusion callers, with a sensitivity of 0.27 for B-ALL gene fusions. Notably, FUSILLI detected *ETV6*::*RUNX1* in three samples, *BCR*::*ABL1* in one sample, and *IGH*::*EPOR* in one sample, which other fusion callers missed. However, as expected, most fusions were undetected because of lower depth of sequencing. The *in silico*, read-depth, subsampling study shows increasing read depth to 10 million reads optimizes fusion detection performance in terms of overall F1 score when requiring a minimum of two supporting reads to call fusions. Likely, increasing sequencing depth beyond the 11.2 million mean read count in the high-depth cohort would provide more support for fusions that were missed, as mentioned above.

Although FUSILLI detects most B-ALL gene fusions in the high-depth cohort, fusion callers' evaluations presented in this study are a result of a limited set of fusion subtypes. Testing on other fusion subtypes, such as *IGH*::*DUX4*, *KMT2A*r, and *ZNF384*r, would provide a more comprehensive evaluation of clinically relevant B-ALL gene fusion detection. Additionally, discerning between *bona fide* B-ALL fusions and chimeric reads stemming from technical and/or computational methods can be challenging. Ambiguous alignments can result from aligning to repetitive regions of the genome. Identifying these repetitive sequences through software, such as RepeatMasker, may improve specificity in repetitive regions.[39] Although longer reads ostensibly lead to better detection of gene fusions (especially those whose breakpoints are far from the poly-A tail of a transcript), a more robust assessment (supplemented by additional data) of average read length or N50 needed to detect specific fusions is needed. For example, in the high-depth cohort, two of the three samples whose *BCR*::*ABL1* fusions were undetected showed average read lengths between 233 and 246 bp compared with correctly detected *BCR*::*ABL1* fusions whose samples ranged in read length from 249 to 796 bp. However, another *BCR*::*ABL1* sample (with no supporting reads for the given fusion) had an

average read length of 251 bp. Investigating the effects of both coverage and read length on fusion detection is needed to provide more definitive guidance on sufficient read lengths resulting from ONT-WTS. FUSILLI also relies on high-depth sequencing (from RNA extraction and PCR-amplified full-length cDNA) and direct fusion detection by looking for reads spanning genes of interest. In contrast, previous work based on gene expression profiling has shown promise in classifying B-ALL genomic subgroups.[34,40]

FUSILLI offers a targeted approach to detecting common, clinically relevant B-ALL gene fusions based on ONT-WTS. With an average high read depth of 11.2 million reads, FUSILLI shows higher sensitivity, outperforming general-purpose fusion callers. Further investigation of detected fusions shows detection of *PAX5*::*ZCCHC7* secondary alterations as well as supplemental fusions requiring further examination. However, read depths below 10 million reads affect sensitivity, limiting the detection of important B-ALL gene fusions. Therefore, FUSILLI's performance is dependent on read depth. Future work will focus on incorporating FUSILLI's algorithmic approach into a general-purpose leukemia classifier, enhancing significant leukemic lineage determinations and the classification of B-ALL genomic subtypes.[34]

Acknowledgment

Figures 1 to 3 in this article were generated using BioRender.com (Toronto, ON, Canada).

Disclosure Statement

None declared.

Supplemental Data

Supplemental material for this article can be found at *https://doi.org/10.1016/j.jmoldx.2026.01.007*.

References

1. Cronin KA, Scott S, Firth AU, Sung H, Henley SJ, Sherman RL, Siegel RL, Anderson RN, Kohler BA, Benard SVB, Negoita S, Wiggins C, Cance WG, Jemal A: Annual report to the nation on the status of cancer, part 1: national cancer statistics. Cancer 2022, 128: 4251−4284
2. Liu YF, Wang BY, Zhang WN, Huang JY, Li BS, Zhang M, et al: Genomic profiling of adult and pediatric B-cell acute lymphoblastic leukemia. EBioMedicine 2016, 8:173−183
3. Inaba H, Pui CH: Advances in the diagnosis and treatment of pediatric acute lymphoblastic leukemia. J Clin Med 2021, 10:1926
4. Cario G, Leoni V, Conter V, Baruchel A, Schrappe M, Biondi A: BCR-ABL1-like acute lymphoblastic leukemia in childhood and targeted therapy. Haematologica 2020, 105:2200−2204
5. Panuciak K, Nowicka E, Mastalerczyk A, Zawitkowska J, Niedźwiecki M, Lejman M: Overview on aneuploidy in childhood B-cell acute lymphoblastic leukemia. Int J Mol Sci 2023, 24:8764
6. Alaggio R, Amador C, Anagnostopoulos I, Attygalle AD, Araujo IBO, Berti E, et al: The 5th edition of the World Health Organization classification of haematolymphoid tumours: lymphoid neoplasms. Leukemia 2022, 36:1720−1748
7. Iacobucci I, Kimura S, Mullighan CG: Biologic and therapeutic implications of genomic alterations in acute lymphoblastic leukemia. J Clin Med 2021, 10:3792
8. Roberts KG, Mullighan CG: The biology of B-progenitor acute lymphoblastic leukemia. Cold Spring Harb Perspect Med 2020, 10: a034835
9. Kansal R: Diagnosis and molecular pathology of lymphoblastic leukemias and lymphomas in the era of genomics and precision medicine: historical evolution and current concepts—part 3: mature leukemias/lymphomas. Lymphatics 2023, 1:155−219
10. Danielson DT, Wendzel NC, Knollmann-Ritschel B, Muir JM: Educational case: diagnostic studies for B-cell acute lymphoblastic leukemia. Acad Pathol 2022, 9:100045
11. Hu T, Chitnis N, Monos D, Dinh A: Next-generation sequencing technologies: an overview. Hum Immunol 2021, 82:801−811
12. Logsdon GA, Vollger MR, Eichler EE: Long-read human genome sequencing and its applications. Nat Rev Genet 2020, 21:597−614
13. Leggett RM, Clark MD: A world of opportunities with nanopore sequencing. J Exp Bot 2017, 68:5419−5429
14. Walter W, Shahswar R, Stengel A, Meggendorfer M, Kern W, Haferlach T, Haferlach C: Clinical application of whole transcriptome sequencing for the classification of patients with acute lymphoblastic leukemia. BMC Cancer 2021, 21:886
15. Bařinka J, Hu Z, Wang L, Wheeler DA, Rahbarinia D, McLeod C, Go Z, Mullighan CG: RNAseqCNV: analysis of large-scale copy number variations from RNA-seq data. Leukemia 2022, 36: 1492−1498
16. Hu Z, Jia Z, Liu J, Mao A, Han H, Gu Z: MD-ALL: an integrative platform for molecular diagnosis of B-acute lymphoblastic leukemia. Haematologica 2024, 109:1741−1754
17. Schmidt B, Brown LM, Ryland GL, Lonsdale A, Kosasih HJ, Ludlow LE, Majewski IJ, Blombery P, Ekert PG, Davidson NM, Oshlack A: ALLSorts: an RNA-seq subtype classifier for B-cell acute lymphoblastic leukemia. Blood Adv 2022, 6:4093−4097
18. Chen Y, Wang Y, Chen W, Tan Z, Song Y; Human Genome Structural Variation Consortium, Chen H, Chong Z: Gene fusion detection and characterization in long-read cancer transcriptome sequencing data with fusionseeker. Cancer Res 2023, 83:28−33
19. Davidson NM, Chen Y, Sadras T, Ryland GL, Blombery P, Ekert PG, Goke J, Oshlack A: JAFFAL: detecting fusion genes with long-read transcriptome sequencing. Genome Biol 2022, 23:10
20. Liu Q, Hu Y, Stucky A, Fang L, Zhong JF, Wang K: LongGF: computational algorithm and software tool for fast and accurate detection of gene fusions by long-read transcriptome sequencing. BMC Genomics 2020, 21:793
21. Twisk DV, Vincent B, Rubinsteyn A: Comparing long read fusion callers using simulated read data. bioRxiv 2022, [Preprint], https://doi.org/10.1101/2022.09.23.509226
22. Gu Z, Churchman ML, Roberts KG, Moore I, Zhou X, Nakitandwe J, et al: PAX5-driven subtypes of B-progenitor acute lymphoblastic leukemia. Nat Genet 2019, 51:296−307
23. Brady SW, Roberts KG, Gu Z, Shi L, Pounds S, Pei D, et al: The genomic landscape of pediatric acute lymphoblastic leukemia. Nat Genet 2022, 54:1376−1389
24. Wick RR, Judd LM, Wyres KL, Holt KE: Recovery of small plasmid sequences via Oxford Nanopore sequencing. Microb Genomics 2021, 7:000631
25. White R, Pellefigues C, Ronchese F, Lamiable O, Eccles D: Investigation of chimeric reads using the MinION. F1000Res 2017, 6:631
26. De Coster W, Rademakers R: NanoPack2: population-scale evaluation of long-read sequencing data. Bioinformatics 2023, 39:btad311

27. Jia Z, Gu Z: PAX5 alterations in B-cell acute lymphoblastic leukemia. Front Oncol 2022, 12:1023606
28. Iacobucci I, Lonetti A, Paoloni F, Papayannidis C, Ferrari A, Storlazzi CT, Vignetti M, Cilloni D, Messa F, Guagagnuolo V, Paolini S, Elia L, Messina M, Vitale A, Meloni G, Soverini S, Pane F, Baccarani M, Foa R, Martinellu G: The PAX5 gene is frequently rearranged in BCR-ABL1-positive acute lymphoblastic leukemia but is not associated with outcome: a report on behalf of the GIMEMA acute leukemia working party. Haematologica 2010, 95:1683
29. Li Y, Zhang Q, Shao H: Recurrent PAX5::ZCCHC7 rearrangement in B-cell acute lymphoblastic leukemia. Ann Hematol 2024, 103: 5599−5605
30. Geyer J, Opoku KB, Lin J, Ramkissoon L, Mullighan C, Bhakta N, Alexander TB, Wang JR: Real-time genomic characterization of pediatric acute leukemia using adaptive sampling. Leukemia 2025, 39:1069−1077
31. Vesely C, Frech C, Eckert C, Cario G, Mecklenbräuker A, Zur Stadt U, Nebral K, Kraler F, Fisher S, Attarbaschi A, Schuster M, Bock C, Cave H, von Stackelberg A, Schrappe M, Hirtsmann MA, Mann G, Hass OA, Panzer-Grumayer R: Genomic and transcriptional landscape of P2RY8-CRLF2-positive childhood acute lymphoblastic leukemia. Leukemia 2017, 31:1491
32. Cario G, Zimmermann M, Romey R, Gesk S, Vater I, Harbott J, Schrauder A, Moericke A, Izaraeli S, Akasaka T, Dyer MJS, Siebert R, Schrappe M, Stanulla M: Presence of the P2RY8-CRLF2 rearrangement is associated with a poor prognosis in non−high-risk precursor B-cell acute lymphoblastic leukemia in children treated according to the ALL-BFM 2000 protocol. Blood 2010, 115: 5393−5397
33. Russell LJ, Jones L, Enshaei A, Tonin S, Ryan SL, Eswaran J, Nakjang S, Papaemmanuil E, Tubio JM, Fielding AK, Vora A, Campbell PJ, Moorman AV, Harrison CJ: Characterisation of the genomic landscape of CRLF2-rearranged acute lymphoblastic leukemia. Genes Chromosomes Cancer 2017, 56:363
34. Wang J, Bhakta N, Ayer Miller V, Revsine M, Litzow MR, Paietta E, Fedoriw Y, Roberts KG, Gu Z, Mullighan CG, Jones CD, Alexander TB: Acute leukemia classification using transcriptional profiles from low-cost nanopore mRNA sequencing. JCO Precis Oncol 2022, 6:e2100326
35. Monzó C, Liu T, Conesa A: Transcriptomics in the era of long-read sequencing. Nat Rev Genet 2025, 26:681−701
36. Adnan-Awad S, Kim D, Hohtari H, Javarappa KK, Brandstoetter T, Mayer I, Potdar S, Heckman CA, Kytola S, Porkka K, Doma E, Sexl V, Kankainen M, Mustjoki S: Characterization of p190-Bcr-Abl chronic myeloid leukemia reveals specific signaling pathways and therapeutic targets. Leukemia 2021, 35:1964−1975
37. Randolph TR: 32: Myeloproliferative neoplasms. Edited by Keohane EM, Otto CN, Walenga JM. In Rodak's Hematology. 6th ed. St. Louis, MO: Elsevier, 2020. pp. 555−588
38. Schebesta A, McManus S, Salvagiotto G, Delogu A, Busslinger GA, Busslinger M: Transcription factor Pax5 activates the chromatin of key genes involved in B cell signaling, adhesion, migration, and immune function. Immunity 2007, 27:49−63
39. Flynn JM, Hubley R, Goubert C, Rosen J, Clark AG, Feschotte C, Smit AF: RepeatModeler2 for automated genomic discovery of transposable element families. Proc Natl Acad Sci U S A 2020, 117: 9451−9457
40. Chiaretti S, Zini G, Bassan R: Diagnosis and subclassification of acute lymphoblastic leukemia. Mediterr J Hematol Infect Dis 2014, 6:e2014073